Design of Unbalanced Mach–Zehnder Interferometers for Waveguide Group Index Extraction

MandanaJim

***Abstract*—This proposal designs and models unbalanced silicon Mach–Zehnder interferometers (MZIs) to extract waveguide group index from the measured free spectral range (FSR). We define the waveguide geometry, simulate guided TE modes, and compute $n_{\text{eff}}(\lambda)$ and $n_g(\lambda)$. A compact polynomial model for $n_{\text{eff}}(\lambda)$ and an analytical MZI transfer function are used to predict transmission spectra across design variants spanning waveguide width and mZI path imbalance ΔL. Expected FSRs are summarized in a DOE (design of experiments) table. A circuit model in INTERCONNECT is built to simulate the transmission spectra and compare with the analytical prediction. The n_g–FSR relationship is also derived so that the group index can be extracted from subsequent experimental measurement given design variants of ΔL and waveguide widths.**

I. Introduction

Silicon photonics enables dense, CMOS-compatible integration of optical waveguides and passive components on silicon-on-insulator (SOI), supporting scalable transceivers and wavelength-division multiplexing systems with compact footprints and high-volume manufacturability [1]. Accurate knowledge of waveguide dispersion—especially the group index $n_g(\lambda)$—is essential for predicting interferometer periodicity, phase sensitivity, delay, and bandwidth in circuits such as filters, sensors, and coherent links [2]. However, $n_g(\lambda)$ depends on waveguide geometry and fabrication variations, motivating an experimental extraction method that can be directly compared to simulation.

The objective of this design proposal is to design an unbalanced interferometer whose transmission fringes provide a direct measurement of $n_g(\lambda)$ via the free spectral range (FSR). We will (i) select waveguide widths, (ii) simulate TE mode profiles and compute $n_{\text{eff}}(\lambda)$ and $n_g(\lambda)$, (iii) develop compact dispersion models for circuit-level prediction, and (iv) choose practical values of ΔL and waveguide width such that the resulting FSR is resolvable with the available measurement setup. The final outcome is a set of MZI design variants and a validated simulation-to-extraction workflow to be applied to measured spectra.

II. Theory

A Mach–Zehnder interferometer (MZI) splits an input optical field into two arms that accumulate different phases and then recombine. For a guided mode with effective index $n_{\text{eff}}(\lambda)$, the propagation constant is

$$\beta(\lambda) = \frac{2\pi}{\lambda}\, n_{\text{eff}}(\lambda). \tag{1}$$

Let the arm lengths be L_1 and L_2, with imbalance

$$\Delta L = L_2 - L_1. \tag{2}$$

The differential phase is

$$\Delta\phi(\lambda) = \beta_2(\lambda)L_2 - \beta_1(\lambda)L_1 + \phi_{\text{off}}, \tag{3}$$

where ϕ_{off} captures any constant phase offset (e.g., splitter phase or small asymmetries). In this proposal both arms use the same cross-section and materials and differ only in length, so

$$\beta_2(\lambda) = \beta_1(\lambda) = \beta(\lambda), \tag{4}$$

and therefore

$$\Delta\phi(\lambda) = \beta(\lambda)\Delta L + \phi_{\text{off}}. \tag{5}$$

For an ideal MZI with 50/50 splitters and negligible loss imbalance, the normalized transmission is

$$T(\lambda) = \frac{1}{2}\left[1 + \cos\big(\Delta\phi(\lambda)\big)\right]. \tag{6}$$

More generally, unequal arm amplitudes reduce contrast but do not change the fringe periodicity:

$$T(\lambda) = T_0 + T_1 \cos\big(\Delta\phi(\lambda)\big). \tag{7}$$

In the following derivation we neglect loss and set ϕ_{off} to zero (or absorb it into the integer fringe index).

Transmission maxima occur when

$$\Delta\phi(\lambda_m) = 2\pi m, \qquad m \in \mathbb{Z}, \tag{8}$$

so that

$$\beta(\lambda_m)\Delta L = 2\pi m. \tag{9}$$

For adjacent maxima at λ_m and $\lambda_{m+1} = \lambda_m + \Delta\lambda$ (with $\text{FSR}_\lambda \equiv \Delta\lambda$),

$$\big[\beta(\lambda_{m+1}) - \beta(\lambda_m)\big]\Delta L = 2\pi. \tag{10}$$

For small $\Delta\lambda$,

$$\beta(\lambda_{m+1}) - \beta(\lambda_m) \approx \frac{d\beta}{d\lambda}\Delta\lambda, \tag{11}$$

hence

$$\frac{d\beta}{d\lambda}\,\text{FSR}_\lambda\,\Delta L \approx 2\pi. \tag{12}$$

With $\beta(\lambda) = \frac{2\pi}{\lambda} n_{\text{eff}}(\lambda)$,

$$\frac{d\beta}{d\lambda} = -\frac{2\pi}{\lambda^2}\left(n_{\text{eff}} - \lambda \frac{dn_{\text{eff}}}{d\lambda}\right) = -\frac{2\pi}{\lambda^2} n_g(\lambda), \quad (13)$$

where

$$n_g(\lambda) = n_{\text{eff}}(\lambda) - \lambda \frac{dn_{\text{eff}}}{d\lambda}. \quad (14)$$

Using magnitudes,

$$\text{FSR}_\lambda \approx \frac{\lambda^2}{n_g(\lambda)\Delta L}, \quad (15)$$

and therefore

$$n_g(\lambda) \approx \frac{\lambda^2}{\text{FSR}_\lambda \, \Delta L}. \quad (16)$$

This first-order approximation assumes (i) dispersion does not vary significantly across one fringe period, (ii) ΔL is accurately known from layout, and (iii) the observed fringes correspond to a single guided mode.

III. Modelling and Simulation

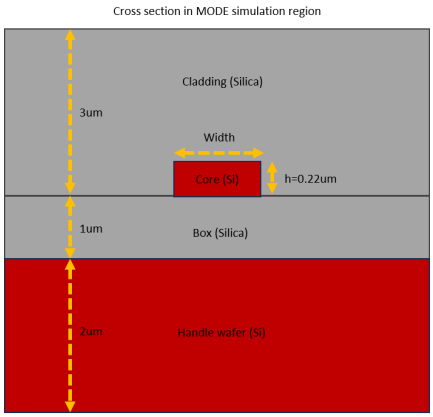

Figure 1. Waveguide cross-section geometry: silicon core thickness $h = 220$ nm and width $w \in \{400, 500, 600\}$ nm.

This section summarizes the modeling workflow and simulation results used to predict the dispersion and spectral response of the designed interferometer circuits prior to measurement. We begin by defining the waveguide and circuit geometries and numerically extracting the wavelength-dependent effective index and group index, $n_{\text{eff}}(\lambda)$ and $n_g(\lambda)$, which are plotted with respect to wavelength. The simulated dispersion is then reduced to a compact polynomial waveguide model that enables efficient circuit-level calculations. Using this compact model, we formulate the device transfer function(s) and simulate the expected transmission spectrum(s) for one or more photonic circuits. A DOE (design of experiment) table is included to document the design splits (e.g., waveguide widths and path-length imbalance ΔL) and to quantify how the predicted free spectral range (FSR) changes with ΔL and waveguide widths.

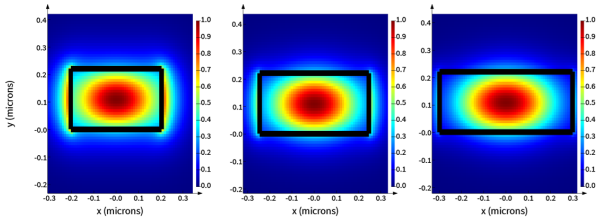

Figure 2. Simulated fundamental waveguide mode profile from Lumerical MODE for width $w \in \{400, 500, 600\}$ nm.

Figure 1 summarizes the assumed SOI strip-waveguide cross section used throughout the simulations, with fixed silicon thickness $h = 220$ nm and three candidate widths $w \in \{400, 500, 600\}$ nm. This geometric definition is the starting point for the eigenmode calculations because it sets the modal confinement and the wavelength dependence of the propagation constant. To verify the guided mode used for dispersion extraction, Fig. 2 shows the simulated fundamental mode profile (e.g., $|E(x, y)|^2$) from Lumerical MODE Solutions; this plot is used to confirm the intended polarization, the expected field confinement in the silicon core, and that the simulated mode is physically reasonable before proceeding to wavelength sweeps.

Table I
DOE of waveguide width and MZI path-length imbalance with simulated group index and expected FSR.

w (nm)	ΔL (μm)	n_g	n_{eff}	$FSR(nm)$
400	100	4.397	2.226	5.464
400	200	4.397	2.226	2.732
400	400	4.397	2.226	1.366
500	100	4.205	2.444	5.713
500	200	4.205	2.444	2.857
500	400	4.205	2.444	1.428
600	100	4.066	2.565	5.909
600	200	4.066	2.565	2.954
600	400	4.066	2.565	1.477

The design-of-experiments (DOE) for the interferometer circuits is summarized in Table I. For each width w, three imbalance lengths ΔL are selected to span a practical range of FSR values while remaining compatible with layout and test constraints. The table records the corresponding simulated indices (n_g and n_{eff}) used for prediction and provides a clear bookkeeping reference for which geometries map to which expected spectral periods. In particular, the FSR estimates in the final column (computed via $\text{FSR}_\lambda \approx \lambda_0^2/(n_g \, \Delta L)$ at $\lambda_0 = 1550$ nm) enable a quick sanity check that the chosen ΔL values produce resolvable fringes over the available measurement bandwidth.

To enable fast circuit-level prediction without re-running full-wave mode simulations, we constructed a compact dispersion model for the waveguide by fitting the simulated effective index to a second-order polynomial over the operating wavelength band. Specifically, the numerically extracted $n_{\text{eff}}(\lambda)$ data (from Lumerical MODE Solutions and/or MATLAB) were least-squares fitted using a Taylor expansion about a center wavelength λ_0,

$$n_{\text{eff}}(\lambda) = n_1 + n_2\,(\lambda - \lambda_0) + n_3\,(\lambda - \lambda_0)^2\,. \qquad (17)$$

With this parameterization, the conventional waveguide quantities at λ_0 follow directly as $n_{\text{eff}}(\lambda_0) = n_1$ and $n_g(\lambda_0) = n_1 - n_2\lambda_0$, while the dispersion parameter is given by $D = -2\lambda_0 n_3/c$ (in $\mathrm{s/m^2}$). The resulting compact, differentiable description of waveguide dispersion is then used in the interferometer phase model $\Delta\phi(\lambda) = \beta(\lambda)\Delta L$, enabling efficient transfer-function simulations that closely match the underlying numerical results across the wavelength range of interest.

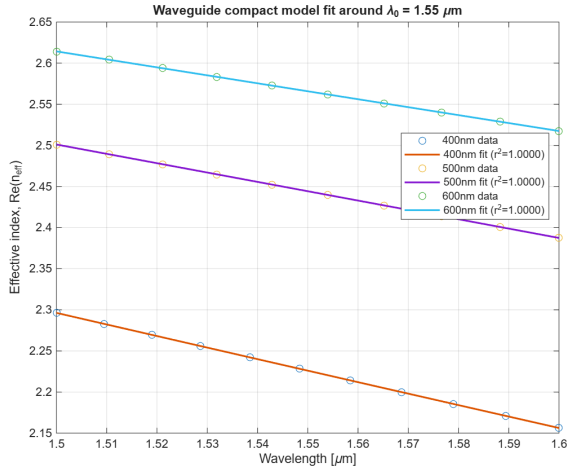

Figure 3. Simulated $n_{\text{eff}}(\lambda)$ (markers) and quadratic compact-model fits (lines) for waveguide widths of 400, 500, and 600 nm, using $n_{\text{eff}}(\lambda) = n_1 + n_2(\lambda - \lambda_0) + n_3(\lambda - \lambda_0)^2$ with $\lambda_0 = 1.55$ μm.

The fitted polynomial coefficients provide a compact summary of the simulated dispersion and are reported in Table II for each width. In addition to the raw fit parameters (n_1, n_2, n_3), the table lists the derived group index $n_g(\lambda_0)$ and dispersion parameter D at λ_0 to facilitate direct comparison across geometries. Figure 4 visualizes the underlying wavelength sweeps of $n_{\text{eff}}(\lambda)$ and $n_g(\lambda)$, while Fig. 4 (compact-model fit) confirms that the quadratic model captures the simulated $n_{\text{eff}}(\lambda)$ trends with excellent agreement over the wavelength span of interest. These plots serve as both a validation of the compact model and as inputs to the subsequent phase and transfer-function calculations.

Using the extracted dispersion and compact-model coefficients, the wavelength-dependent propagation constant is evaluated as $\beta(\lambda) = 2\pi n_{\text{eff}}(\lambda)/\lambda$, and the interferometer phase difference is computed via $\Delta\phi(\lambda) = \beta(\lambda)\Delta L$. The resulting transfer function(s) are then used to generate predicted transmission spectra for each circuit variant. Figure 5 overlays the simulated transmission responses $T(\lambda)$, enabling a direct visual comparison of how the spectral periodicity (FSR) changes with ΔL and how the waveguide width (through n_g and dispersion) shifts the fringe spacing and spectral alignment. This spectral overlay is particularly useful for selecting a subset of devices that provide well-separated FSRs for

Table II
WAVEGUIDE COMPACT MODEL COEFFICIENTS FROM QUADRATIC FIT $n_{\text{eff}}(\lambda) = n_1 + n_2(\lambda - \lambda_0) + n_3(\lambda - \lambda_0)^2$ (WITH λ IN μM).

	400	**500**	**600**
n_1	2.2260	2.4443	2.5658
n_2 ($\mu\mathbf{m}^{-1}$)	-1.4000	-1.1364	-0.9683
n_3 ($\mu\mathbf{m}^{-2}$)	1.015×10^{-1}	-1.466×10^{-3}	2.941×10^{-2}
$n_g(\lambda_0)$	4.3960	4.2057	4.0667
D ($\mathbf{s/m}^2$)	-1.050×10^{-15}	1.516×10^{-17}	-3.041×10^{-16}

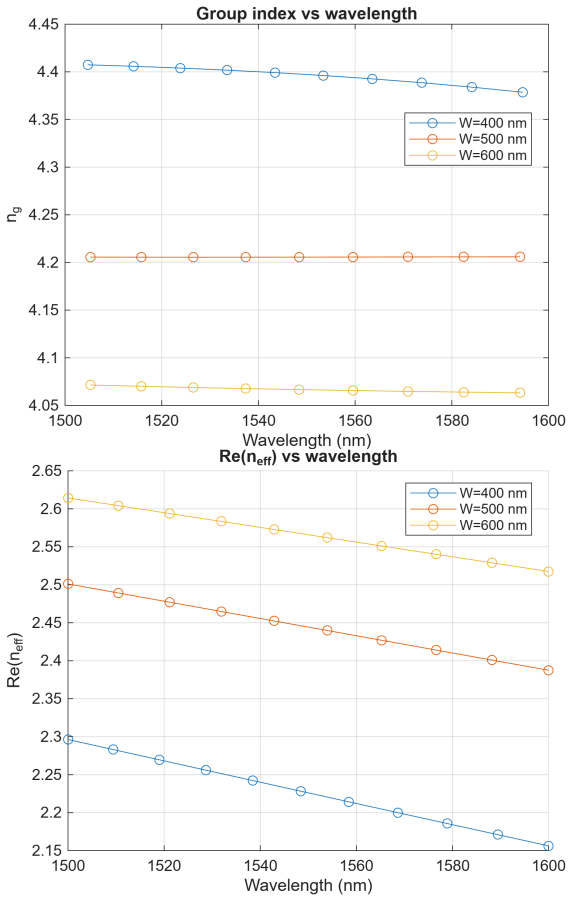

Figure 4. Simulated waveguide dispersion: (top) effective index $n_{\text{eff}}(\lambda)$ and (bottom) group index $n_g(\lambda)$ versus wavelength for width $w \in \{400, 500, 600\}$ nm.

robust group-index extraction in subsequent measurements.

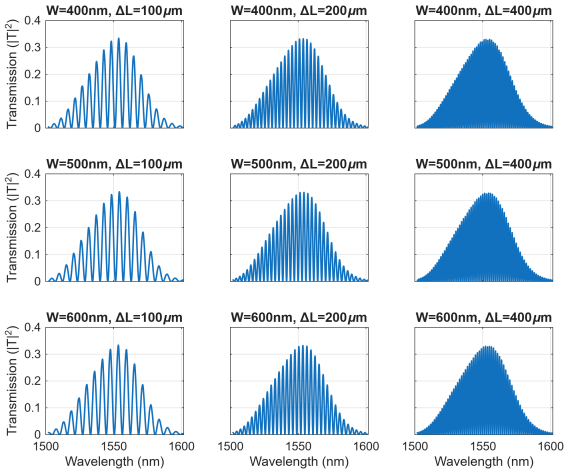

Figure 5. Simulated transmission spectra in Interconnect $T(\lambda)$ for 3 length and 3 width variants. The envelope is a result of the input/output grating couplers

IV. Fabrication

This section will be completed in the final report.

V. Experimental Data

This section will be completed in the final report.

VI. Analysis

This section will be completed in the final report.

VII. Conclusion

This section will be completed in the final report.

VIII. Acknowledgements

This section will be completed in the final report.

References

1. Chrostowski L, Hochberg M (2015) Silicon Photonics Design. Cambridge University Press (CUP)

2. Bojko RJ, Li J, He L, et al. (2011) Electron beam lithography writing strategies for low loss high confinement silicon optical waveguides. Journal of Vacuum Science & Technology B: Microelectronics and Nanometer Structures 29:06F309. https://doi.org/10.1116/1.3653266

3. Chrostowski L, Hochberg M Testing and packaging. In: Silicon Photonics Design. Cambridge University Press (CUP), pp 381–405

4. Wang Y, Wang X, Flueckiger J, et al. (2014) Focusing sub-wavelength grating couplers with low back reflections for rapid prototyping of silicon photonic circuits. Opt Express 22:20652. https://doi.org/10.1364/oe.22.020652